Design and application of wavelet-based refinement criteria for hyperbolic conservation laws within the AMROC mesh adaptation framework

Ralf Deiterding* and Margarete O. Domingues†

*Aerodynamics and Flight Mechanics Research Group
University of Southampton
Highfield Campus, Southampton SO17 1BJ, UK
E-mail: r.deiterding@soton.ac.uk

†INPE - National Institute for Space Research
LAC/CTE
Sao Jose dos Campos, Brazil

September 21, 2017

Outline

Principles of SAMR
- Block-structured adaptive mesh refinement
- Common refinement criteria
- Implementation in AMROC

Multiresolution techniques
- Multiresolution principles
- New MR refinement criteria

Computational results for Euler equations
- Verification
- Lax–Liu test cases

Computational results for magneto-hydrodynamics
- Ideal magneto-hydrodynamics simulation

Conclusions
- Summary and outlook

Collaboration with

- Kai Schneider and Oliver Roussel (University of Marseille, France)
- Muller Moreira Lopes (INPE – LAC/CTE)

Block-structured adaptive mesh refinement (SAMR)

For simplicity $\partial_t \mathbf{q}(\mathbf{x},t) + \nabla \cdot \mathbf{f}(\mathbf{q}(\mathbf{x},t)) = 0$

- Refined blocks overlay coarser ones

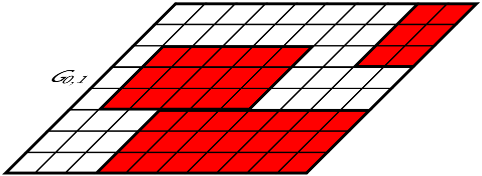

Block-structured adaptive mesh refinement (SAMR)

For simplicity $\partial_t \mathbf{q}(\mathbf{x}, t) + \nabla \cdot \mathbf{f}(\mathbf{q}(\mathbf{x}, t)) = 0$

- Refined blocks overlay coarser ones

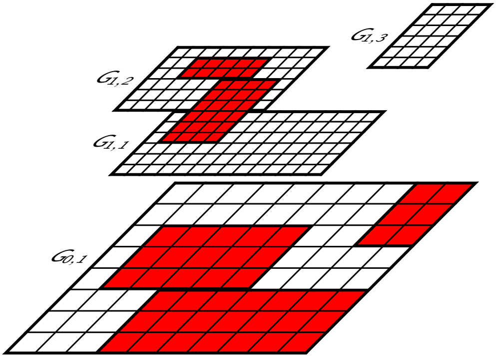

Block-structured adaptive mesh refinement (SAMR)

For simplicity $\partial_t \mathbf{q}(\mathbf{x},t) + \nabla \cdot \mathbf{f}(\mathbf{q}(\mathbf{x},t)) = 0$

- Refined blocks overlay coarser ones

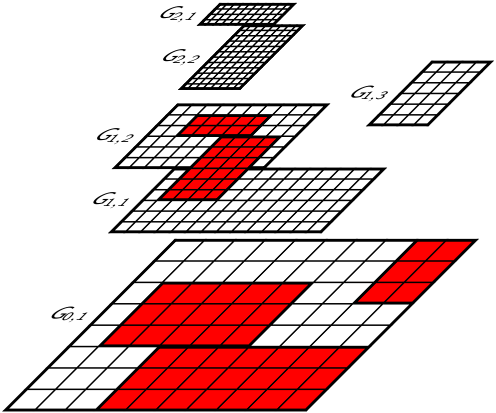

Block-structured adaptive mesh refinement (SAMR)

For simplicity $\partial_t \mathbf{q}(\mathbf{x},t) + \nabla\cdot\mathbf{f}(\mathbf{q}(\mathbf{x},t)) = 0$

- Refined blocks overlay coarser ones
- Refinement in space *and time* by factor r_l
- Block (aka patch) based data structures

+ Numerical scheme

$$\mathbf{Q}_{jk}^{n+1} = \mathbf{Q}_{jk}^{n} - \frac{\Delta t}{\Delta x}\left[\mathbf{F}_{j+\frac{1}{2},k} - \mathbf{F}_{j-\frac{1}{2},k}\right] - \frac{\Delta t}{\Delta y}\left[\mathbf{G}_{j,k+\frac{1}{2}} - \mathbf{G}_{j,k-\frac{1}{2}}\right]$$

  only for single patch necessary

+ Efficient cache-reuse / vectorization possible

- Cluster-algorithm necessary

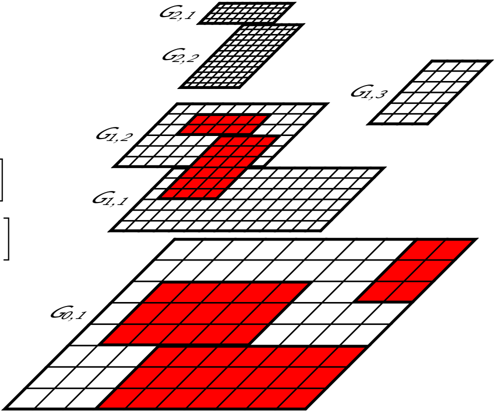

Level transfer / setting of ghost cells

Conservative averaging (restriction):

$$\hat{\mathbf{Q}}^{l}_{jk} := \frac{1}{(r_{l+1})^2} \sum_{\kappa=0}^{r_{l+1}-1} \sum_{\iota=0}^{r_{l+1}-1} \mathbf{Q}^{l+1}_{v+\kappa, w+\iota}$$

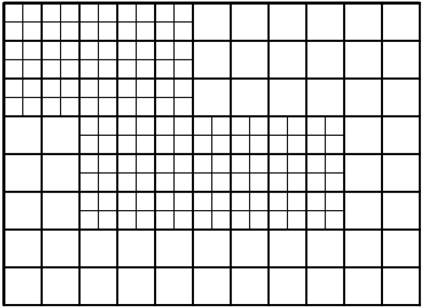

Level transfer / setting of ghost cells

Conservative averaging (restriction):

$$\hat{\mathbf{Q}}^{l}_{jk} := \frac{1}{(r_{l+1})^2} \sum_{\kappa=0}^{r_{l+1}-1} \sum_{\iota=0}^{r_{l+1}-1} \mathbf{Q}^{l+1}_{v+\kappa,w+\iota}$$

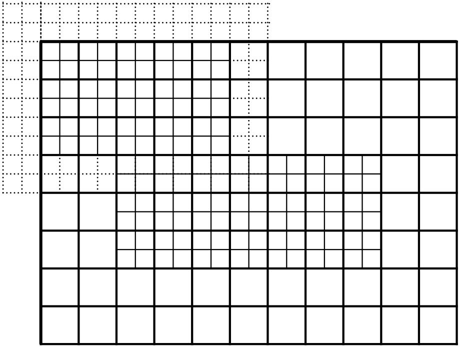

Level transfer / setting of ghost cells

Conservative averaging (restriction):

$$\hat{\mathbf{Q}}^{l}_{jk} := \frac{1}{(r_{l+1})^2} \sum_{\kappa=0}^{r_{l+1}-1} \sum_{\iota=0}^{r_{l+1}-1} \mathbf{Q}^{l+1}_{v+\kappa,w+\iota}$$

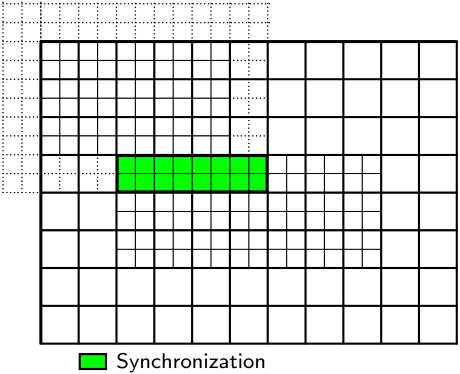

Level transfer / setting of ghost cells

Conservative averaging (restriction):

$$\hat{\mathbf{Q}}^l_{jk} := \frac{1}{(r_{l+1})^2} \sum_{\kappa=0}^{r_{l+1}-1} \sum_{\iota=0}^{r_{l+1}-1} \mathbf{Q}^{l+1}_{v+\kappa,w+\iota}$$

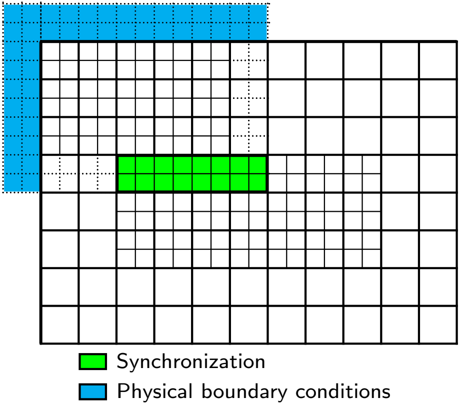

Level transfer / setting of ghost cells

Conservative averaging (restriction):

$$\hat{\mathbf{Q}}^{l}_{jk} := \frac{1}{(r_{l+1})^2} \sum_{\kappa=0}^{r_{l+1}-1} \sum_{\iota=0}^{r_{l+1}-1} \mathbf{Q}^{l+1}_{v+\kappa,w+\iota}$$

Bilinear interpolation (prolongation):

$$\check{\mathbf{Q}}^{l+1}_{vw} := (1-f_1)(1-f_2)\,\mathbf{Q}^{l}_{j-1,k-1} + f_1(1-f_2)\,\mathbf{Q}^{l}_{j,k-1} + (1-f_1)f_2\,\mathbf{Q}^{l}_{j-1,k} + f_1 f_2\,\mathbf{Q}^{l}_{jk}$$

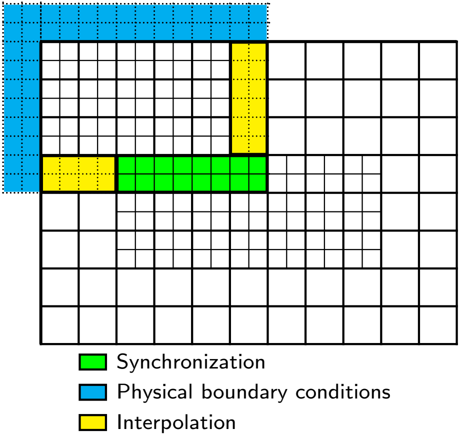

For boundary conditions: linear time interpolation

$$\tilde{\mathbf{Q}}^{l+1}(t+\kappa\Delta t_{l+1}) := \left(1-\frac{\kappa}{r_{l+1}}\right)\check{\mathbf{Q}}^{l+1}(t) + \frac{\kappa}{r_{l+1}}\check{\mathbf{Q}}^{l+1}(t+\Delta t_l) \quad \text{for } \kappa = 0, \ldots r_{l+1}$$

Conservative flux correction

Example: Cell j, k

$$\check{\mathbf{Q}}^l_{jk}(t+\Delta t_l) = \mathbf{Q}^l_{jk}(t) - \frac{\Delta t_l}{\Delta x_l}\left(\mathbf{F}^{1,l}_{j+\frac{1}{2},k} - \frac{1}{r^2_{l+1}}\sum_{\kappa=0}^{r_{l+1}-1}\sum_{\iota=0}^{r_{l+1}-1}\mathbf{F}^{1,l+1}_{v+\frac{1}{2},w+\iota}(t+\kappa\Delta t_{l+1})\right) - \frac{\Delta t_l}{\Delta y_l}\left(\mathbf{F}^{2,l}_{j,k+\frac{1}{2}} - \mathbf{F}^{2,l}_{j,k-\frac{1}{2}}\right)$$

Correction pass:

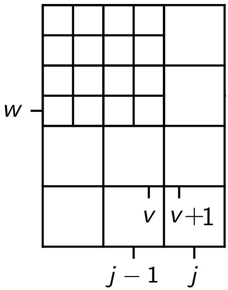

Conservative flux correction

Example: Cell j, k

$$\check{\mathbf{Q}}^l_{jk}(t+\Delta t_l) = \mathbf{Q}^l_{jk}(t) - \frac{\Delta t_l}{\Delta x_l}\left(\mathbf{F}^{1,l}_{j+\frac{1}{2},k} - \frac{1}{r^2_{l+1}} \sum_{\kappa=0}^{r_{l+1}-1} \sum_{\iota=0}^{r_{l+1}-1} \mathbf{F}^{1,l+1}_{v+\frac{1}{2},w+\iota}(t+\kappa\Delta t_{l+1})\right) - \frac{\Delta t_l}{\Delta y_l}\left(\mathbf{F}^{2,l}_{j,k+\frac{1}{2}} - \mathbf{F}^{2,l}_{j,k-\frac{1}{2}}\right)$$

Correction pass:

1. $\delta \mathbf{F}^{1,l+1}_{j-\frac{1}{2},k} := -\mathbf{F}^{1,l}_{j-\frac{1}{2},k}$

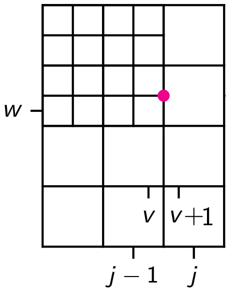

Conservative flux correction

Example: Cell j, k

$$\check{\mathbf{Q}}^l_{jk}(t+\Delta t_l) = \mathbf{Q}^l_{jk}(t) - \frac{\Delta t_l}{\Delta x_l}\left(\mathbf{F}^{1,l}_{j+\frac{1}{2},k} - \frac{1}{r^2_{l+1}}\sum_{\kappa=0}^{r_{l+1}-1}\sum_{\iota=0}^{r_{l+1}-1}\mathbf{F}^{1,l+1}_{v+\frac{1}{2},w+\iota}(t+\kappa\Delta t_{l+1})\right) - \frac{\Delta t_l}{\Delta y_l}\left(\mathbf{F}^{2,l}_{j,k+\frac{1}{2}} - \mathbf{F}^{2,l}_{j,k-\frac{1}{2}}\right)$$

Correction pass:

1. $\delta\mathbf{F}^{1,l+1}_{j-\frac{1}{2},k} := -\mathbf{F}^{1,l}_{j-\frac{1}{2},k}$
2. $\delta\mathbf{F}^{1,l+1}_{j-\frac{1}{2},k} := \delta\mathbf{F}^{1,l+1}_{j-\frac{1}{2},k} + \frac{1}{r^2_{l+1}}\sum_{\iota=0}^{r_{l+1}-1}\mathbf{F}^{1,l+1}_{v+\frac{1}{2},w+\iota}(t+\kappa\Delta t_{l+1})$

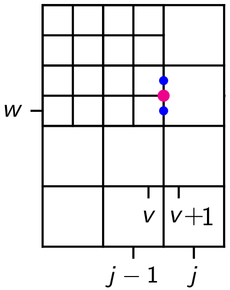

Conservative flux correction

Example: Cell j, k

$$\check{\mathbf{Q}}^l_{jk}(t+\Delta t_l) = \mathbf{Q}^l_{jk}(t) - \frac{\Delta t_l}{\Delta x_l}\left(\mathbf{F}^{1,l}_{j+\frac{1}{2},k} - \frac{1}{r^2_{l+1}}\sum_{\kappa=0}^{r_{l+1}-1}\sum_{\iota=0}^{r_{l+1}-1}\mathbf{F}^{1,l+1}_{v+\frac{1}{2},w+\iota}(t+\kappa\Delta t_{l+1})\right) - \frac{\Delta t_l}{\Delta y_l}\left(\mathbf{F}^{2,l}_{j,k+\frac{1}{2}} - \mathbf{F}^{2,l}_{j,k-\frac{1}{2}}\right)$$

Correction pass:

1. $\delta\mathbf{F}^{1,l+1}_{j-\frac{1}{2},k} := -\mathbf{F}^{1,l}_{j-\frac{1}{2},k}$
2. $\delta\mathbf{F}^{1,l+1}_{j-\frac{1}{2},k} := \delta\mathbf{F}^{1,l+1}_{j-\frac{1}{2},k} + \frac{1}{r^2_{l+1}}\sum_{\iota=0}^{r_{l+1}-1}\mathbf{F}^{1,l+1}_{v+\frac{1}{2},w+\iota}(t+\kappa\Delta t_{l+1})$
3. $\check{\mathbf{Q}}^l_{jk}(t+\Delta t_l) := \mathbf{Q}^l_{jk}(t+\Delta t_l) + \frac{\Delta t_l}{\Delta x_l}\,\delta\mathbf{F}^{1,l+1}_{j-\frac{1}{2},k}$

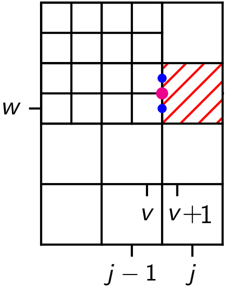

Refinement criteria

Scaled gradient of scalar quantity w

$$|w(\mathbf{Q}_{j+1,k})-w(\mathbf{Q}_{jk})| > \epsilon_w\ ,\ |w(\mathbf{Q}_{j,k+1})-w(\mathbf{Q}_{jk})| > \epsilon_w\ ,\ |w(\mathbf{Q}_{j+1,k+1})-w(\mathbf{Q}_{jk})| > \epsilon_w$$

Refinement criteria

Scaled gradient of scalar quantity w

$$|w(\mathbf{Q}_{j+1,k})-w(\mathbf{Q}_{jk})| > \epsilon_w \;,\; |w(\mathbf{Q}_{j,k+1})-w(\mathbf{Q}_{jk})| > \epsilon_w \;,\; |w(\mathbf{Q}_{j+1,k+1})-w(\mathbf{Q}_{jk})| > \epsilon_w$$

2. Create temporary Grid coarsened by factor 2

   Initialize with fine-grid-values of preceding time step

1. Richardson-type error estimation on interior cells

3. Compare temporary solutions

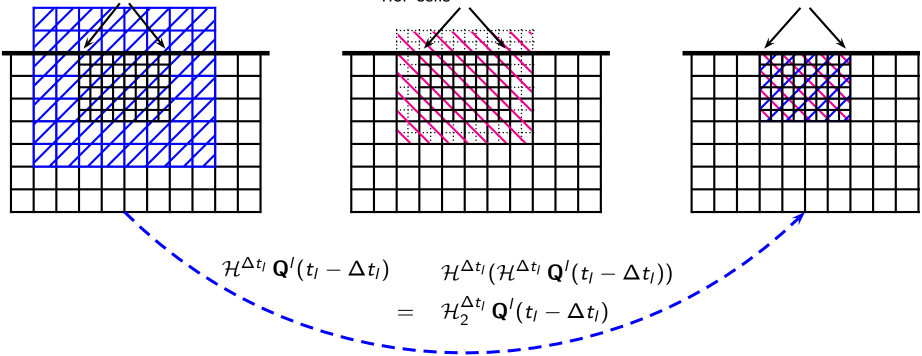

$$\mathcal{H}^{\Delta t_l}\,\mathbf{Q}^l(t_l-\Delta t_l)$$

$$\begin{aligned}&\mathcal{H}^{\Delta t_l}(\mathcal{H}^{\Delta t_l}\,\mathbf{Q}^l(t_l-\Delta t_l))\\ =\;&\mathcal{H}_2^{\Delta t_l}\,\mathbf{Q}^l(t_l-\Delta t_l)\end{aligned}$$

$$\mathcal{H}^{2\Delta t_l}\,\bar{\mathbf{Q}}^l(t_l-\Delta t_l)$$

UML design of AMROC

- Classical framework approach with generic main program in C++

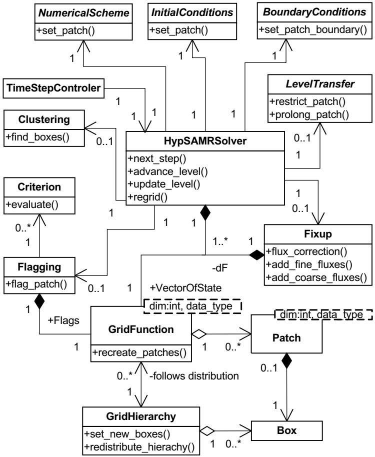

UML design of AMROC

- Classical framework approach with generic main program in C++
- Customization / modification in Problem.h include file by derivation from base classes and redefining virtual interface functions

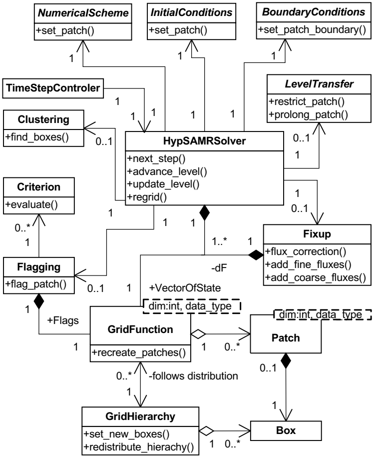

UML design of AMROC

- Classical framework approach with generic main program in C++
- Customization / modification in Problem.h include file by derivation from base classes and redefining virtual interface functions
- Predefined, scheme-specific classes provided for standard simulations

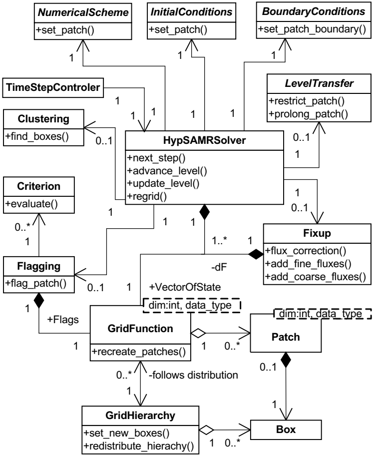

Multiresolution (MR) principles

- Multiresolution analysis is a tool to construct wavelet functions and consequently wavelet transforms
  - Information can be organized in different scale levels
  - Scale can be associated to periods bands
- Information in a certain level can be obtained by the combination of the coarser levels with the wavelet coefficient contributions and vice-versa

$$\mathbf{Q}^{\ell+1} \underset{\textit{prediction}}{\overset{\textit{projection}}{\rightleftharpoons}} \mathbf{Q}_{\mathrm{MR}}^{\ell+1} = \{\mathbf{Q}^{\ell}\} \cup \{d^{\ell}\},$$

Multiresolution (MR) principles

- Multiresolution analysis is a tool to construct wavelet functions and consequently wavelet transforms
  - Information can be organized in different scale levels
  - Scale can be associated to periods bands
- Information in a certain level can be obtained by the combination of the coarser levels with the wavelet coefficient contributions and vice-versa

$$\mathbf{Q}^{\ell+1} \underset{\textit{prediction}}{\overset{\textit{projection}}{\rightleftharpoons}} \mathbf{Q}_{\mathrm{MR}}^{\ell+1} = \{\mathbf{Q}^{\ell}\} \cup \{d^{\ell}\},$$

- PDE approach: **Harten's cell average MR** is used, which is compatible with the underlying FV discretization [Rousell et al., 2003]
- **Wavelet coefficients** are used to characterize the local regularity of the solution
  - low amplitudes of the coefficients are associated to regions where the solution is smooth
  - high amplitudes appear only in regions where the solution is less regular.

MR operations for FV methods

1. Projection (restriction):

$$P_{\ell+1}^{\ell} : \mathbf{Q}^{\ell+1} \rightarrow \mathbf{Q}^{\ell}$$

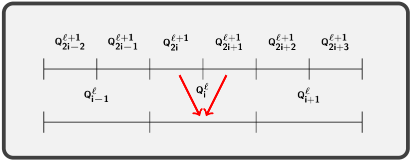

$$P_{\ell+1}^{\ell} : \mathbf{Q}_i^{\ell} = \frac{1}{2}\left(\mathbf{Q}_{2i}^{\ell+1} + \mathbf{Q}_{2i+1}^{\ell+1}\right)$$

2. Prediction (prolongation):

$$P_{\ell}^{\ell+1} : \mathbf{Q}^{\ell} \rightarrow \tilde{\mathbf{Q}}^{\ell+1}$$

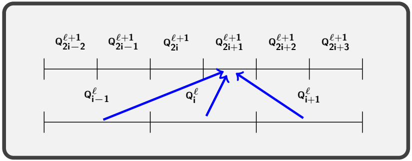

$$P_{\ell,0}^{\ell+1} : \tilde{\mathbf{Q}}_{2i}^{\ell+1} = \mathbf{Q}_i^{\ell} - \frac{1}{8}(\mathbf{Q}_{i+1}^{\ell} - \mathbf{Q}_{i-1}^{\ell}),$$

$$P_{\ell,1}^{\ell+1} : \tilde{\mathbf{Q}}_{2i+1}^{\ell+1} = \mathbf{Q}_i^{\ell} + \frac{1}{8}(\mathbf{Q}_{i+1}^{\ell} - \mathbf{Q}_{i-1}^{\ell})$$

2nd order polynomial interpolation as proposed by [Harten, 1995].

Use of wavelet transform for adaptation

Wavelet coefficients:

$$\boxed{\mathbf{d}^{\ell} = \mathbf{Q}^{\ell+1} - \mathbf{P}_{\ell}^{\ell+1}\,\mathbf{Q}^{\ell} \qquad \text{prediction error}}$$

Use of predicton error as refinement criterion:

$$|\mathbf{Q}^{\ell} - P_{\ell-1}^{\ell}\,P_{\ell}^{\ell-1}\,\mathbf{Q}^{\ell}| > \epsilon$$

Choice of ϵ:

Use of wavelet transform for adaptation

Wavelet coefficients:

$$\boxed{\mathbf{d}^\ell = \mathbf{Q}^{\ell+1} - \mathbf{P}_\ell^{\ell+1}\,\mathbf{Q}^\ell \qquad \text{prediction error}}$$

Use of predicton error as refinement criterion:

$$|\mathbf{Q}^\ell - P_{\ell-1}^{\ell}\,P_\ell^{\ell-1}\,\mathbf{Q}^\ell| > \epsilon$$

Choice of ϵ:

- level-independent threshold parameter $\epsilon \equiv \epsilon_\ell$
- Harten's thresholding strategy:

$$\epsilon^\ell = \frac{\epsilon}{|\Omega|} 2^{2(\ell+1-L)}, \quad 0 \le \ell < L$$

- vector-valued threshold in Eucledian norm of velocity field component of $\mathbf{Q}$

Moving Gaussian bump

- Initial condition:

$$\rho(x,y) = 1 + \exp\left(-\frac{x^2+y^2}{\frac{1}{16}}\right), \; u_x(x,y) = u_y(x,y) \equiv 1, \; p(x,y) \equiv 1$$

- Domain size: $[-1,1] \times [-1,1]$
- Periodic boundary conditions
- The exact solution is a bump moving along the diagonal $x = y$, without changing its shape.
- Base grid of $80 \times 80 + 3$ levels (all refined by a factor 2)
- Finite volume scheme is the Van Leer flux-vector splitting, second order accurate MUSCL slope-limiting method combined with dimensional splitting.
- Clustering efficiency $\eta = 0.95$.
- Final time: $t_e = 2$

Moving Gausian bump - refinement meshes

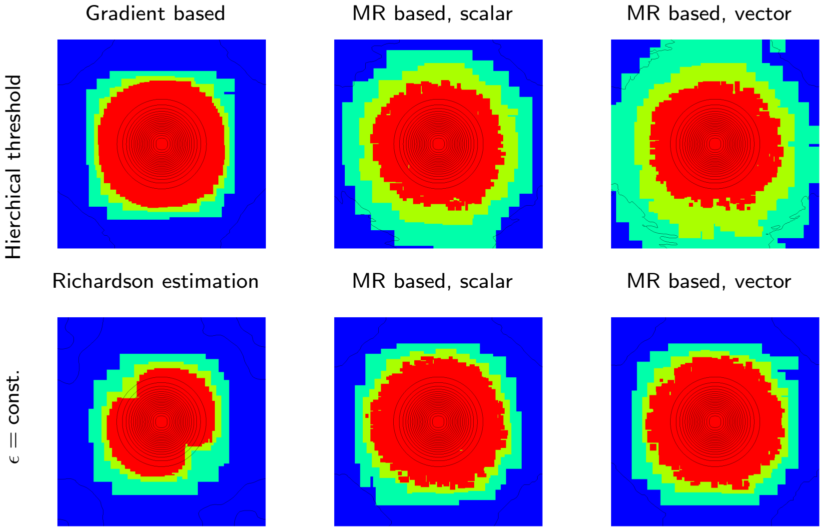

Cells on finest level versus error

L_1^ρ

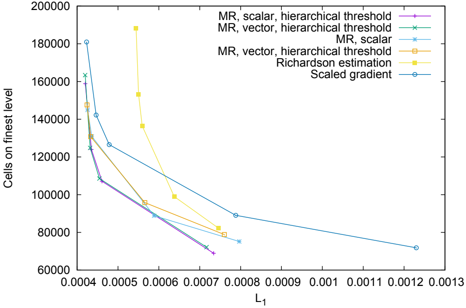

$L_{1,AMR}^\rho$

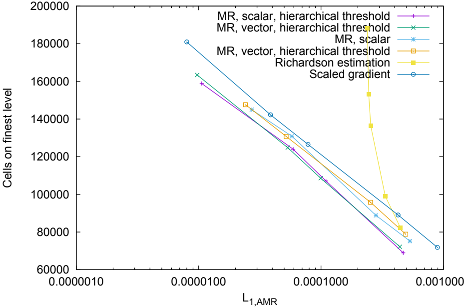

- Level-wise adaptation error: $L_{1,AMR}(\mathbf{Q}, G_\ell) = \sum_{i,j} |\mathbf{Q}_{i,j} - \mathbf{Q}^r_{i,j}| \Delta x_\ell \Delta y_\ell$.
  $\mathbf{Q}^r_{i,j}$ is reference solution from uniform at highest resolution

Cells on finest level versus error

L_1^ρ

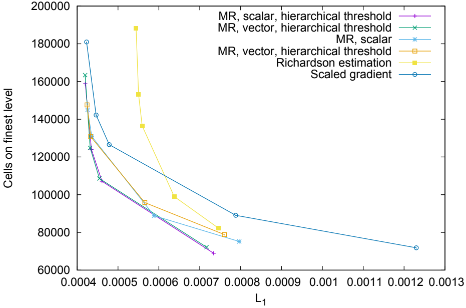

$L_{1,AMR}^\rho$

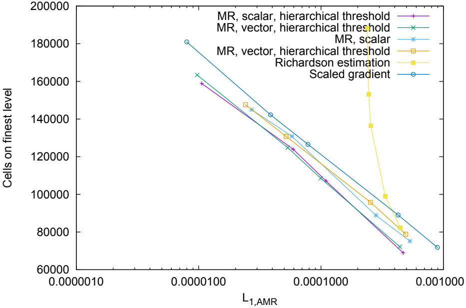

- Level-wise adaptation error: $L_{1,AMR}(\mathbf{Q}, G_\ell) = \sum_{i,j} |\mathbf{Q}_{i,j} - \mathbf{Q}^r_{i,j}| \Delta x_\ell \Delta y_\ell$. $\mathbf{Q}^r_{i,j}$ is reference solution from uniform at highest resolution
- Since the errors satisfy $L_1(\mathbf{Q}) - L_{1,uni}(\mathbf{Q}) \le L_{1,AMR}(\mathbf{Q})$ and $L_{1,uni}$ is a constant, monotone behavior in $L_{1,AMR}$ will be preserved in L_1.

Cells on finest level versus error

L_1^{ρ}

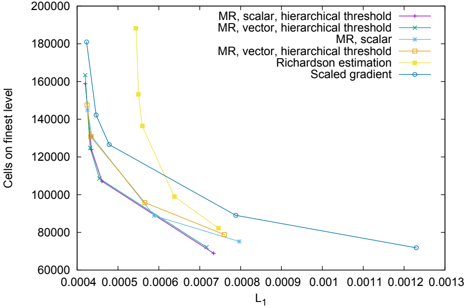

$L_{1,AMR}^{\rho}$

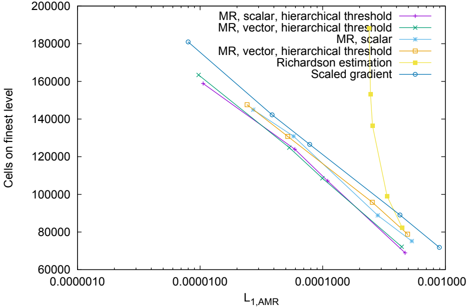

- Level-wise adaptation error: $L_{1,AMR}(\mathbf{Q}, G_\ell) = \sum_{i,j} |\mathbf{Q}_{i,j} - \mathbf{Q}^r_{i,j}| \Delta x_\ell \Delta y_\ell$. $\mathbf{Q}^r_{i,j}$ is reference solution from uniform at highest resolution
- Since the errors satisfy $L_1(\mathbf{Q}) - L_{1,uni}(\mathbf{Q}) \leq L_{1,AMR}(\mathbf{Q})$ and $L_{1,uni}$ is a constant, monotone behavior in $L_{1,AMR}$ will be preserved in L_1.
- all MR criteria are more efficient than the SG and the Richardson estimation criteria

Lax–Liu configurations

Initial Values for the Lax-Liu configuration #6.

Variables	Domain position			
	I	II	III	IV
Density(ρ)	1.00	2.00	1.00	3.00
Pressure (p)	1.00	1.00	1.00	1.00
Velocity component (v_1)	0.75	0.75	-0.75	-0.75
Velocity component (v_2)	-0.50	0.50	0.50	-0.50

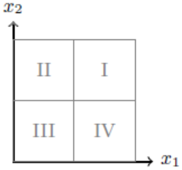

- 2nd-order accurate shock-capturing **MUSCL-Hancock** scheme with **Minmod limiter** and **AUSMDV** flux-vector splitting.
- Base mesh of 8×8 cells, with 8 additional levels refined by factor 2
- Full mesh of 2048×2048 cells, final time of $t_e = 0.8$.
- Left: cluster threshold η also varied. Total number of cells accumulated over all time steps.

$L^{\rho}_{1,AMR}$

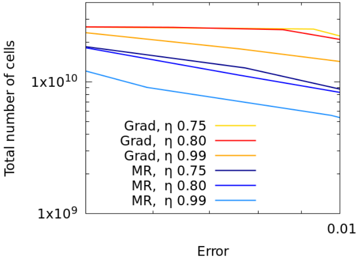

Configuration #6 at $t_e = 0.8$ – Refinement

SAMR with SG criterion, $\epsilon^\rho = 0.05$

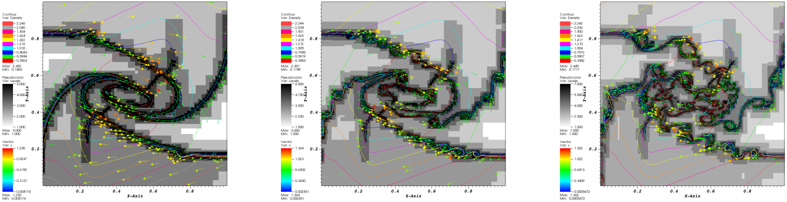

SAMR with MR criterion, $\epsilon = 0.0025$

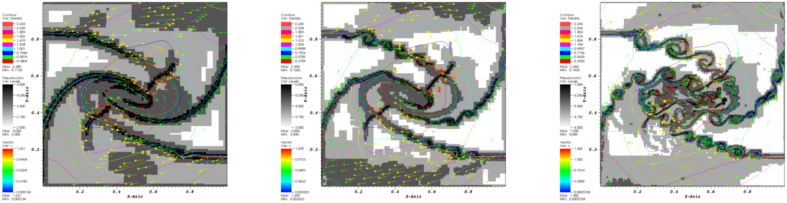

1024^2 2048^2 4096^2

Configuration #3 at $t_e = 0.3$

SG

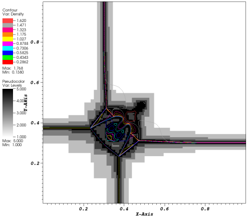

MR

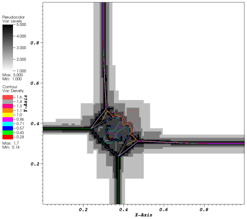

MRV$^+$

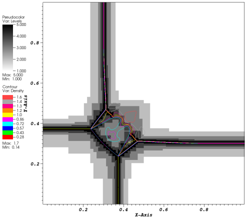

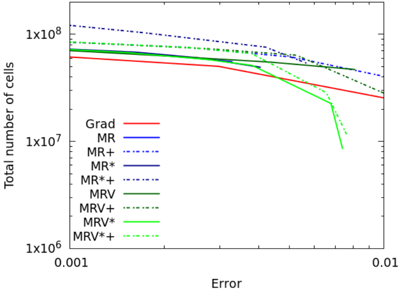

Method	threshold	# of cells (10^7)	$L^{\rho}_{1,AMR}$ (10^{-3})
SG	0.250	5.03	3.0
MR	0.005	6.42	1.9
MR*	0.005	6.83	1.6
MR$^+$	0.010	7.59	2.3
MR$^{*,+}$	0.010	10.35	1.7
MRV	0.010	6.45	1.7
MRV*	0.010	6.76	1.5
MRV$^+$	0.025	7.33	2.8
MRV$^{*,+}$	0.025	7.55	2.3

V: Vector-valued threshold, *: hierchical thresholding, $+$: one buffer cell

Summary of Lax–Liu configuration tests

- We studied 19 configurations at 12 threshold values. For $\eta = 0.8$, the average cell savings of the MR approach versus SG are:

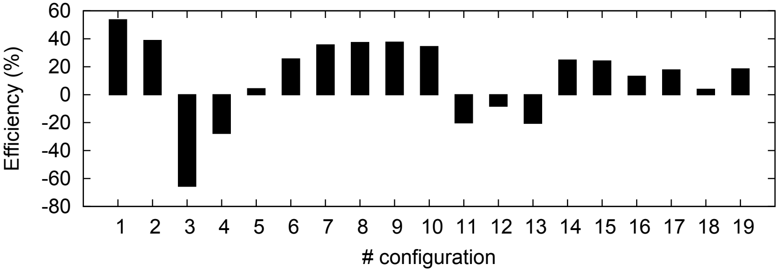

- The majority of configurations involve all three wave types and for those the new MR criteria are most efficient.

Summary of Lax–Liu configuration tests

- We studied 19 configurations at 12 threshold values. For $\eta = 0.8$, the average cell savings of the MR approach versus SG are:

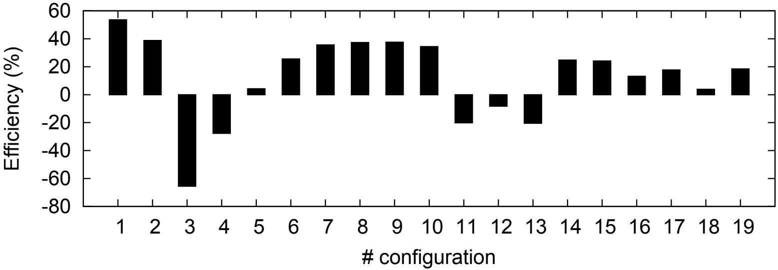

- The majority of configurations involve all three wave types and for those the new MR criteria are most efficient.
- For the few configurations, that are dominated at large by isolated global discontinuites, especially $\#3$, SG can be slightly more effective than MR.

Summary of Lax–Liu configuration tests

- We studied 19 configurations at 12 threshold values. For $\eta = 0.8$, the average cell savings of the MR approach versus SG are:

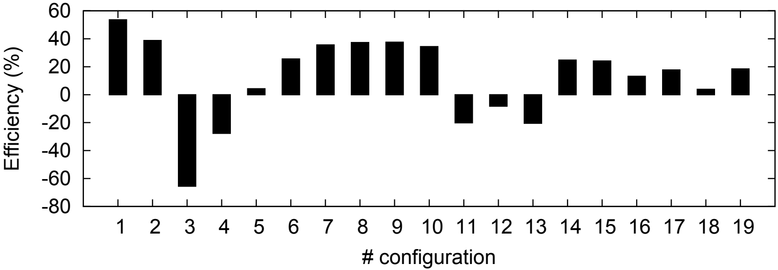

- The majority of configurations involve all three wave types and for those the new MR criteria are most efficient.
- For the few configurations, that are dominated at large by isolated global discontinuites, especially $\#3$, SG can be slightly more effective than MR.
- The simple SG criterion is basically unaffected by numerical artefacts from the FV method, the MR criteria tend to over-refine those

Governing equations

$$\frac{\partial \rho}{\partial t} + \nabla \cdot (\rho \mathbf{u}) = 0$$

$$\frac{\partial \rho \mathbf{u}}{\partial t} + \nabla \cdot \left[\rho \mathbf{u}^{\mathbf{t}} \mathbf{u} + \left(p + \frac{\mathbf{B} \cdot \mathbf{B}}{2} \right) \mathbf{I} - \mathbf{B}^{\mathbf{t}} \mathbf{B} \right] = \mathbf{0}$$

$$\frac{\partial \rho E}{\partial t} + \nabla \cdot \left[\left(\rho E + p + \frac{\mathbf{B} \cdot \mathbf{B}}{2} \right) \mathbf{u} - (\mathbf{u} \cdot \mathbf{B}) \, \mathbf{B} \right] = 0$$

$$\frac{\partial \mathbf{B}}{\partial t} + \nabla \cdot \left(\mathbf{u}^{\mathbf{t}} \mathbf{B} - \mathbf{B}^{\mathbf{t}} \mathbf{u} \right) = \mathbf{0}$$

with equation of state

$$p = (\gamma - 1) \left(\rho E - \rho \frac{\mathbf{u}^2}{2} - \frac{\mathbf{B}^2}{2} \right)$$

The ideal MDH model is still hyperbolic, yet by re-writing the induction equation, one finds that the magnetic field has to satisfy at all times t the elliptic constraint

$$\nabla \cdot \mathbf{B} = 0.$$

Generalized Lagrangian multipliers for divergence control

Hyperbolic-parabolic correction of 2d ideal MHD model [Dedner et al., 2002]:

$$\frac{\partial \rho}{\partial t} + \frac{\partial \rho u_x}{\partial x} + \frac{\partial \rho u_y}{\partial y} = 0$$

$$\frac{\partial (\rho u_x)}{\partial t} + \frac{\partial}{\partial x}\left[\rho u_x^2 + p\left(p + \frac{\mathbf{B}\cdot\mathbf{B}}{2}\right) - B_x^2\right] + \frac{\partial}{\partial y}\left(\rho u_x u_y - B_x B_y\right) = 0$$

$$\frac{\partial (\rho u_y)}{\partial t} + \frac{\partial}{\partial x}\left(\rho u_x u_y - B_x B_y\right) + \frac{\partial}{\partial y}\left[\rho u_y^2 + p\left(p + \frac{\mathbf{B}\cdot\mathbf{B}}{2}\right) - B_y^2\right] = 0$$

$$\frac{\partial (\rho u_z)}{\partial t} + \frac{\partial}{\partial x}\left(\rho u_z u_x - B_z B_x\right) + \frac{\partial}{\partial y}\left(\rho u_z u_y - B_z B_y\right) = 0$$

$$\frac{\partial \rho E}{\partial t} + \frac{\partial}{\partial x}\left[\left(\rho E + p + \frac{\mathbf{B}\cdot\mathbf{B}}{2}\right)\mathbf{u_x} - (\mathbf{u}\cdot\mathbf{B})\, B_x\right] + \frac{\partial}{\partial y}\left[\left(\rho E + p + \frac{\mathbf{B}\cdot\mathbf{B}}{2}\right)\mathbf{u_y} - (\mathbf{u}\cdot\mathbf{B})\, B_y\right] = 0$$

$$\frac{\partial B_x}{\partial t} + \frac{\partial \psi}{\partial x} + \frac{\partial}{\partial y}\left(u_y B_x - B_y u_x\right) = 0$$

$$\frac{\partial B_y}{\partial t} + \frac{\partial}{\partial x}\left(u_x B_y - B_x u_y\right) + \frac{\partial \psi}{\partial y} = 0$$

$$\frac{\partial B_z}{\partial t} + \frac{\partial}{\partial x}\left(u_x B_z - B_z u_x\right) + \frac{\partial}{\partial y}\left(u_y B_z - B_y u_z\right) = 0$$

$$\frac{\partial \psi}{\partial t} + c_h^2\left(\frac{\partial B_x}{\partial x} + \frac{\partial B_y}{\partial y}\right) = -\frac{c_h^2}{c_p^2}\psi$$

Orszag-Tang vortex

- Adaptive solution on 50×50 grid with 4 additional levels refined by $r_l = 2$
- Initial condition

$$\rho(x,y,0) = \gamma^2, \quad u_x(x,y,0) = -\sin(y), \quad u_y(x,y,0) = \sin(x), \quad u_z(x,y,0) = 0$$

$$p(x,y,0) = \gamma, \quad B_x(x,y,0) = -\sin(y), \quad B_y(x,y,0) = 2\sin(x), \quad B_z(x,y,0) = 0$$

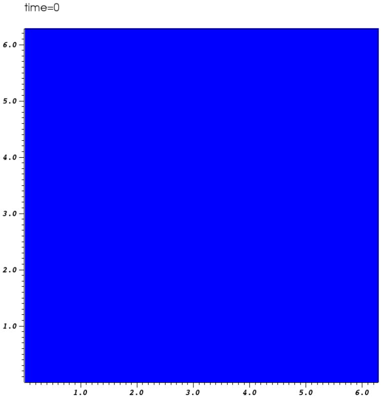

Scaled gradient of ρ

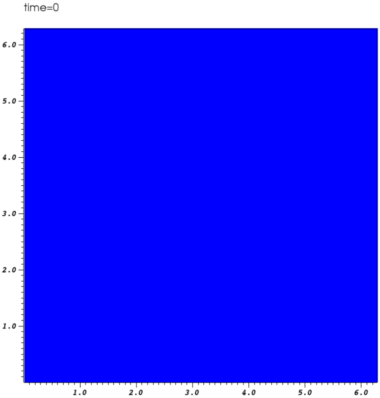

Multi-resolution criterion with hierarchical thresholding

Orszag-Tang vortex

- Adaptive solution on 50×50 grid with 4 additional levels refined by $r_l = 2$
- Initial condition

$$\rho(x,y,0) = \gamma^2, \quad u_x(x,y,0) = -\sin(y), \quad u_y(x,y,0) = \sin(x), \quad u_z(x,y,0) = 0$$
$$p(x,y,0) = \gamma, \quad B_x(x,y,0) = -\sin(y), \quad B_y(x,y,0) = 2\sin(x), \quad B_z(x,y,0) = 0$$

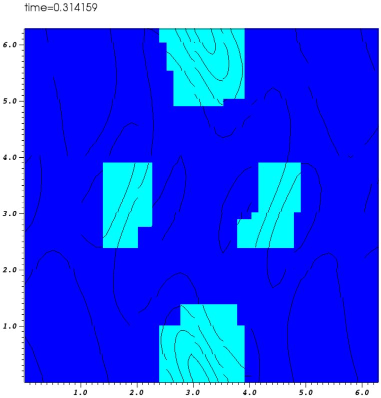

Scaled gradient of ρ

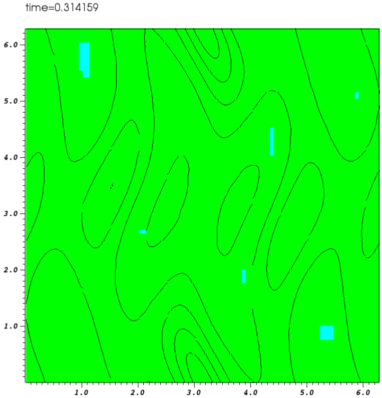

Multi-resolution criterion with hierarchical thresholding

Orszag-Tang vortex

- Adaptive solution on 50×50 grid with 4 additional levels refined by $r_l = 2$
- Initial condition

$$\rho(x,y,0) = \gamma^2, \quad u_x(x,y,0) = -\sin(y), \quad u_y(x,y,0) = \sin(x), \quad u_z(x,y,0) = 0$$

$$p(x,y,0) = \gamma, \quad B_x(x,y,0) = -\sin(y), \quad B_y(x,y,0) = 2\sin(x), \quad B_z(x,y,0) = 0$$

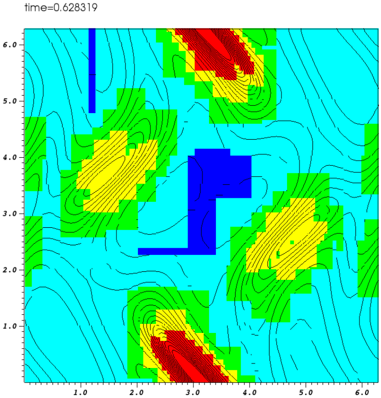

Scaled gradient of ρ

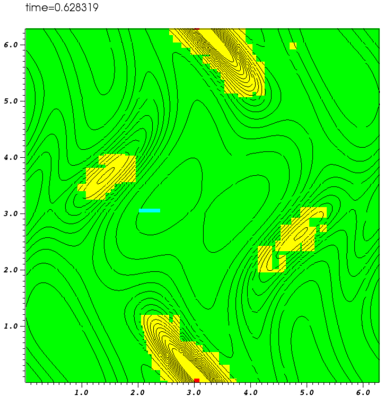

Multi-resolution criterion with hierarchical thresholding

Orszag-Tang vortex

- Adaptive solution on 50×50 grid with 4 additional levels refined by $r_l = 2$
- Initial condition

$$\rho(x,y,0) = \gamma^2, \quad u_x(x,y,0) = -\sin(y), \quad u_y(x,y,0) = \sin(x), \quad u_z(x,y,0) = 0$$

$$p(x,y,0) = \gamma, \quad B_x(x,y,0) = -\sin(y), \quad B_y(x,y,0) = 2\sin(x), \quad B_z(x,y,0) = 0$$

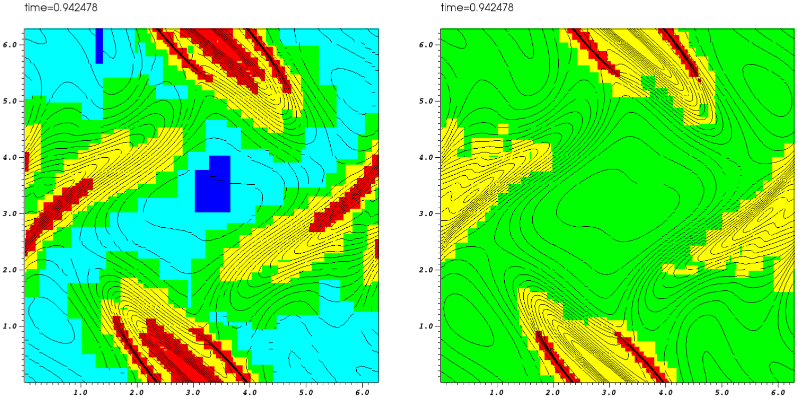

Scaled gradient of ρ — Multi-resolution criterion with hierarchical thresholding

Orszag-Tang vortex

- Adaptive solution on 50×50 grid with 4 additional levels refined by $r_l = 2$
- Initial condition

$$\rho(x,y,0) = \gamma^2, \quad u_x(x,y,0) = -\sin(y), \quad u_y(x,y,0) = \sin(x), \quad u_z(x,y,0) = 0$$
$$p(x,y,0) = \gamma, \quad B_x(x,y,0) = -\sin(y), \quad B_y(x,y,0) = 2\sin(x), \quad B_z(x,y,0) = 0$$

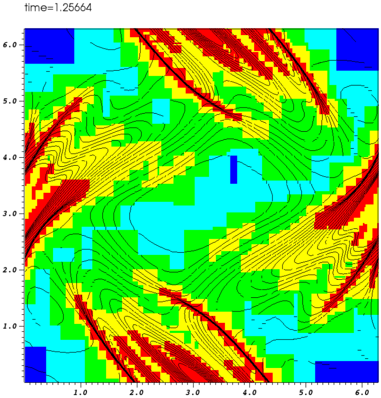

Scaled gradient of ρ

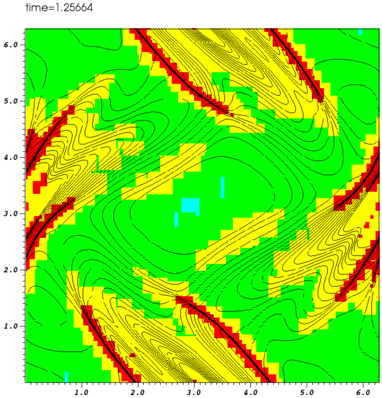

Multi-resolution criterion with hierarchical thresholding

Orszag-Tang vortex

- Adaptive solution on 50×50 grid with 4 additional levels refined by $r_l = 2$
- Initial condition

$$\rho(x,y,0) = \gamma^2, \quad u_x(x,y,0) = -\sin(y), \quad u_y(x,y,0) = \sin(x), \quad u_z(x,y,0) = 0$$

$$p(x,y,0) = \gamma, \quad B_x(x,y,0) = -\sin(y), \quad B_y(x,y,0) = 2\sin(x), \quad B_z(x,y,0) = 0$$

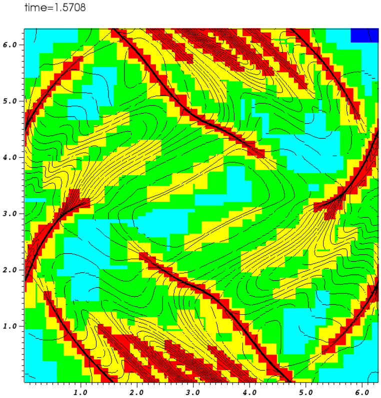

Scaled gradient of ρ

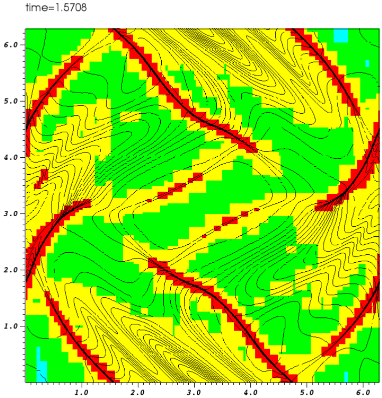

Multi-resolution criterion with hierarchical thresholding

Orszag-Tang vortex

- Adaptive solution on 50×50 grid with 4 additional levels refined by $r_l = 2$
- Initial condition

$$\rho(x,y,0) = \gamma^2, \quad u_x(x,y,0) = -\sin(y), \quad u_y(x,y,0) = \sin(x), \quad u_z(x,y,0) = 0$$

$$p(x,y,0) = \gamma, \quad B_x(x,y,0) = -\sin(y), \quad B_y(x,y,0) = 2\sin(x), \quad B_z(x,y,0) = 0$$

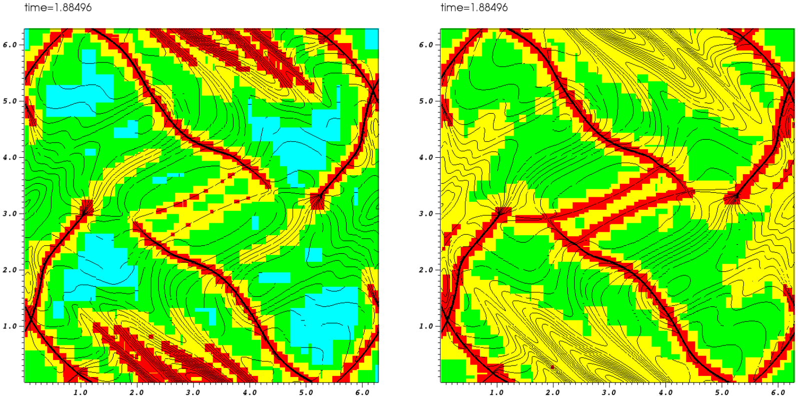

Scaled gradient of ρ | Multi-resolution criterion with hierarchical thresholding

Orszag-Tang vortex

- Adaptive solution on 50×50 grid with 4 additional levels refined by $r_l = 2$
- Initial condition

$$\rho(x,y,0) = \gamma^2, \quad u_x(x,y,0) = -\sin(y), \quad u_y(x,y,0) = \sin(x), \quad u_z(x,y,0) = 0$$
$$p(x,y,0) = \gamma, \quad B_x(x,y,0) = -\sin(y), \quad B_y(x,y,0) = 2\sin(x), \quad B_z(x,y,0) = 0$$

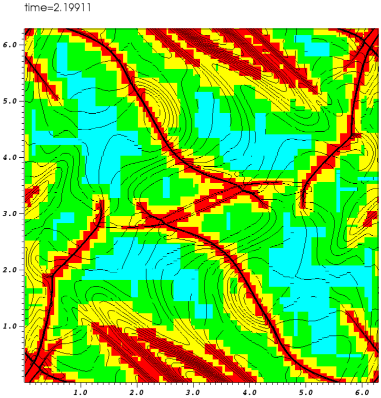

Scaled gradient of ρ

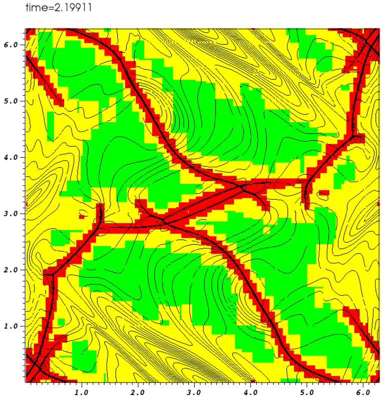

Multi-resolution criterion with hierarchical thresholding

Orszag-Tang vortex

- Adaptive solution on 50×50 grid with 4 additional levels refined by $r_l = 2$
- Initial condition

$$\rho(x,y,0) = \gamma^2, \quad u_x(x,y,0) = -\sin(y), \quad u_y(x,y,0) = \sin(x), \quad u_z(x,y,0) = 0$$

$$p(x,y,0) = \gamma, \quad B_x(x,y,0) = -\sin(y), \quad B_y(x,y,0) = 2\sin(x), \quad B_z(x,y,0) = 0$$

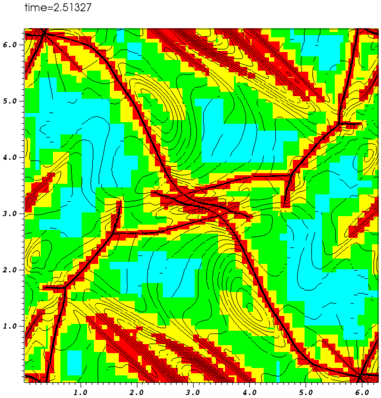

Scaled gradient of ρ

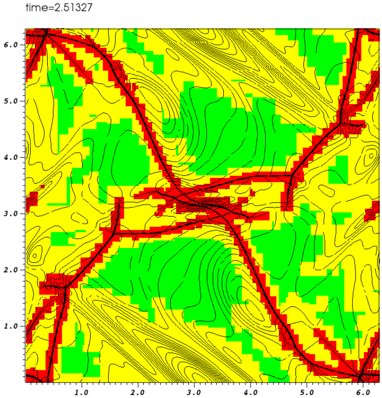

Multi-resolution criterion with hierarchical thresholding

Orszag-Tang vortex

- Adaptive solution on 50×50 grid with 4 additional levels refined by $r_l = 2$
- Initial condition

$$\rho(x,y,0) = \gamma^2, \quad u_x(x,y,0) = -\sin(y), \quad u_y(x,y,0) = \sin(x), \quad u_z(x,y,0) = 0$$

$$p(x,y,0) = \gamma, \quad B_x(x,y,0) = -\sin(y), \quad B_y(x,y,0) = 2\sin(x), \quad B_z(x,y,0) = 0$$

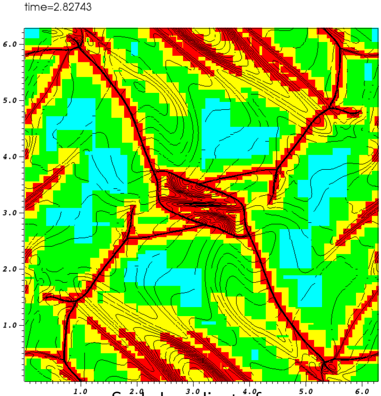

Scaled gradient of ρ

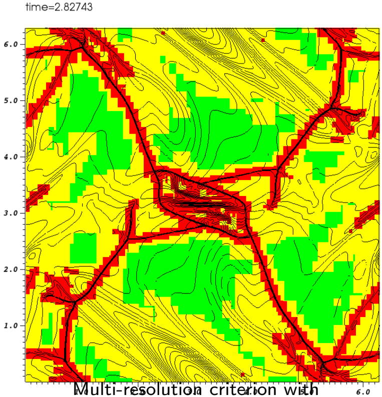

Multi-resolution criterion with hierarchical thresholding

Orszag-Tang vortex

- Adaptive solution on 50×50 grid with 4 additional levels refined by $r_l = 2$
- Initial condition

$$\rho(x,y,0) = \gamma^2, \quad u_x(x,y,0) = -\sin(y), \quad u_y(x,y,0) = \sin(x), \quad u_z(x,y,0) = 0$$

$$p(x,y,0) = \gamma, \quad B_x(x,y,0) = -\sin(y), \quad B_y(x,y,0) = 2\sin(x), \quad B_z(x,y,0) = 0$$

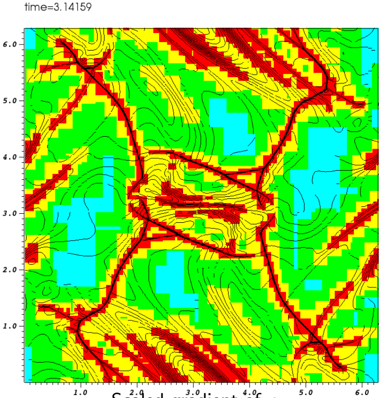

Scaled gradient of ρ

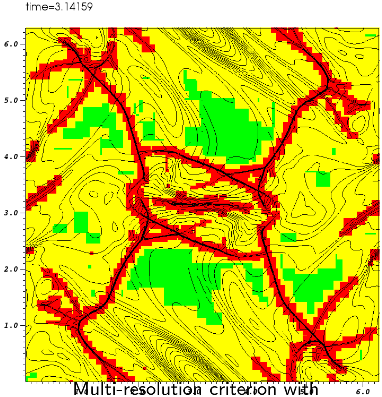

Multi-resolution criterion with hierarchical thresholding

Orszag-Tang vortex - cells on finest level vs. error

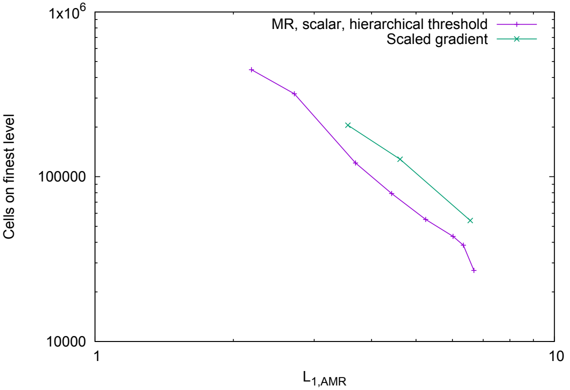

- This is work in progress, and for now, the error is evaluated in ρ only.
- Compared are SG and MR with hierarchical threshold also applied to ρ only.

Orszag-Tang vortex in 3D

- Adaptive solution on $32 \times 32 \times 32$ grid with 3 additional levels refined by $r_l = 2$
- Initial condition

$$\rho(x,y,z) = \gamma^2, \quad p(x,y,0) = \gamma, \quad e = 0.2, \quad \gamma = 5/3, \quad u_z(x,y,z) = e\sin(2\pi z)$$

$$u_x(x,y,z) = -(1 + e\sin(2\pi z))\sin(2\pi y), \quad u_y(x,y,z) = (1 + e\sin(2\pi z))\sin(2\pi x)$$

$$B_x(x,y,z) = -\sin(2\pi y), \quad B_y(x,y,z) = \sin(4\pi x), \quad B_z(x,y,z) = 0$$

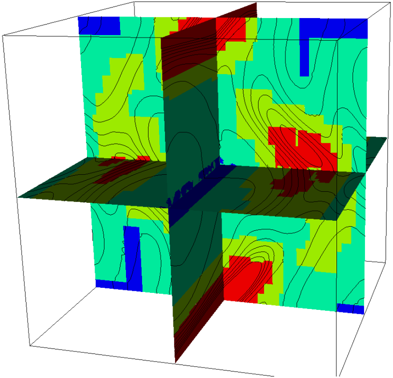

Scaled gradients

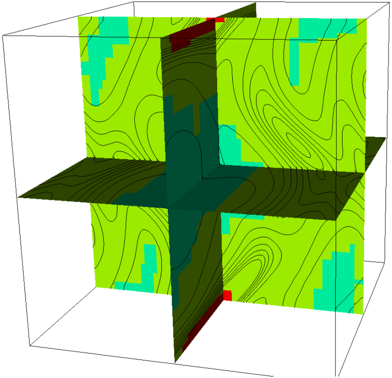

Multi-resolution criteria with hierarchical thresholding

Orszag-Tang vortex in 3D

- Adaptive solution on $32 \times 32 \times 32$ grid with 3 additional levels refined by $r_l = 2$
- Initial condition

$$\rho(x,y,z) = \gamma^2, \quad p(x,y,0) = \gamma, \quad e = 0.2, \quad \gamma = 5/3, \quad u_z(x,y,z) = e\sin(2\pi z)$$
$$u_x(x,y,z) = -(1 + e\sin(2\pi z))\sin(2\pi y), \quad u_y(x,y,z) = (1 + e\sin(2\pi z))\sin(2\pi x)$$
$$B_x(x,y,z) = -\sin(2\pi y), \quad B_y(x,y,z) = \sin(4\pi x), \quad B_z(x,y,z) = 0$$

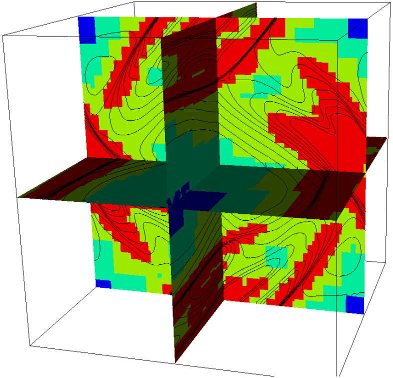

Scaled gradients

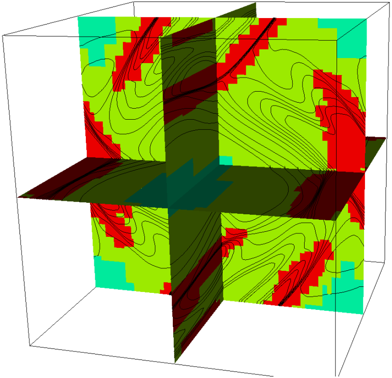

Multi-resolution criteria with hierarchical thresholding

Orszag-Tang vortex in 3D

- Adaptive solution on $32 \times 32 \times 32$ grid with 3 additional levels refined by $r_l = 2$
- Initial condition

$$\rho(x,y,z) = \gamma^2, \quad p(x,y,0) = \gamma, \quad e = 0.2, \quad \gamma = 5/3, \quad u_z(x,y,z) = e\sin(2\pi z)$$

$$u_x(x,y,z) = -(1 + e\sin(2\pi z))\sin(2\pi y), \quad u_y(x,y,z) = (1 + e\sin(2\pi z))\sin(2\pi x)$$

$$B_x(x,y,z) = -\sin(2\pi y), \quad B_y(x,y,z) = \sin(4\pi x), \quad B_z(x,y,z) = 0$$

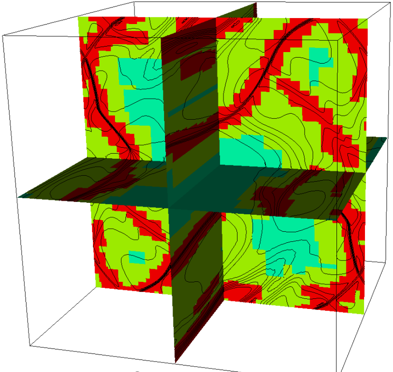

Scaled gradients

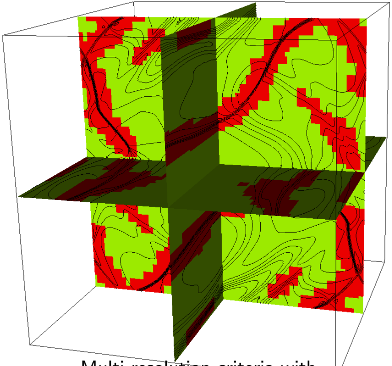

Multi-resolution criteria with hierarchical thresholding

Orszag-Tang vortex in 3D

- Adaptive solution on $32 \times 32 \times 32$ grid with 3 additional levels refined by $r_l = 2$
- Initial condition

$$\rho(x,y,z) = \gamma^2, \quad p(x,y,0) = \gamma, \quad e = 0.2, \quad \gamma = 5/3, \quad u_z(x,y,z) = e\sin(2\pi z)$$

$$u_x(x,y,z) = -(1 + e\sin(2\pi z))\sin(2\pi y), \quad u_y(x,y,z) = (1 + e\sin(2\pi z))\sin(2\pi x)$$

$$B_x(x,y,z) = -\sin(2\pi y), \quad B_y(x,y,z) = \sin(4\pi x), \quad B_z(x,y,z) = 0$$

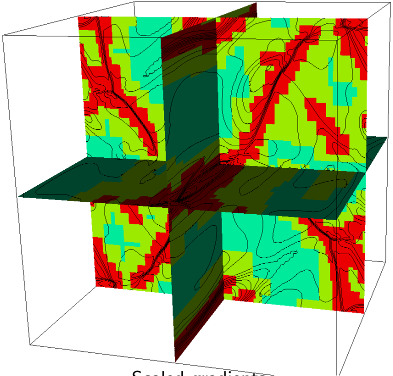

Scaled gradients

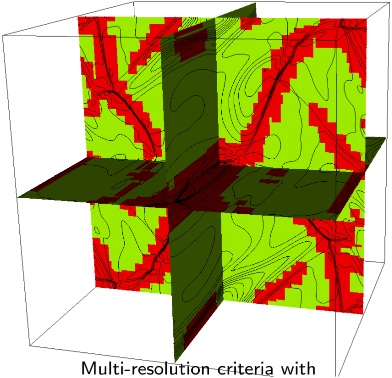

Multi-resolution criteria with hierarchical thresholding

Orszag-Tang vortex in 3D

$t = 0.0$

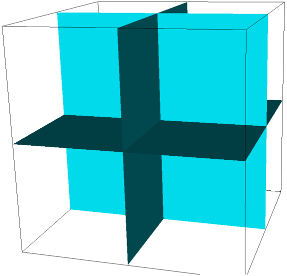

ρ

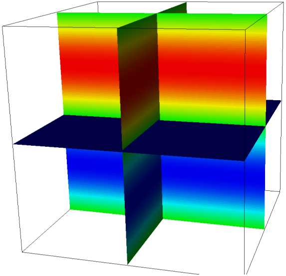

B_x

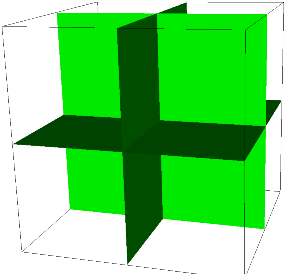

Divergence

Orszag-Tang vortex in 3D

$t = 0.1$

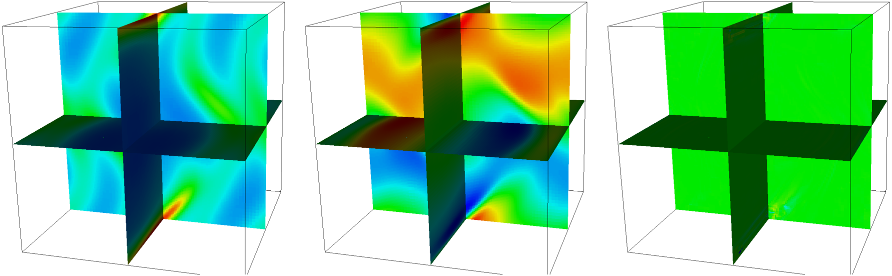

ρ B_x Divergence

Orszag-Tang vortex in 3D

$t = 0.2$

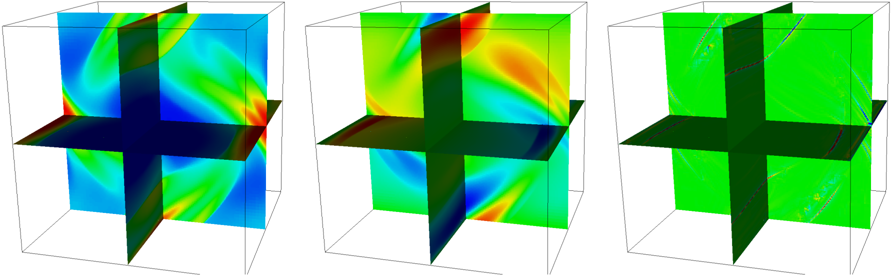

ρ B_x Divergence

Orszag-Tang vortex in 3D

$t = 0.3$

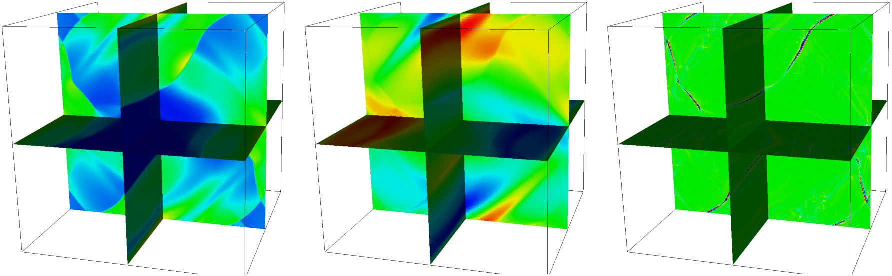

ρ B_x Divergence

Orszag-Tang vortex in 3D

$t = 0.4$

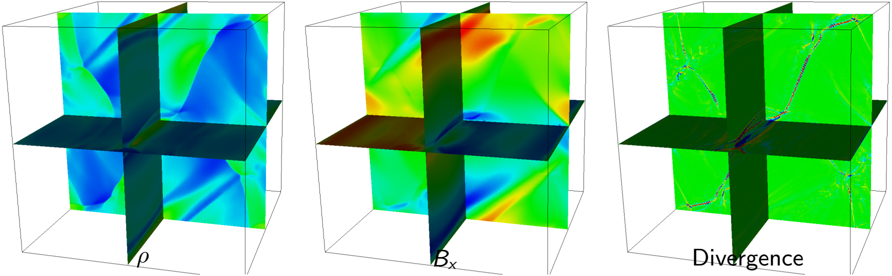

Orszag-Tang vortex in 3D

$t = 0.5$

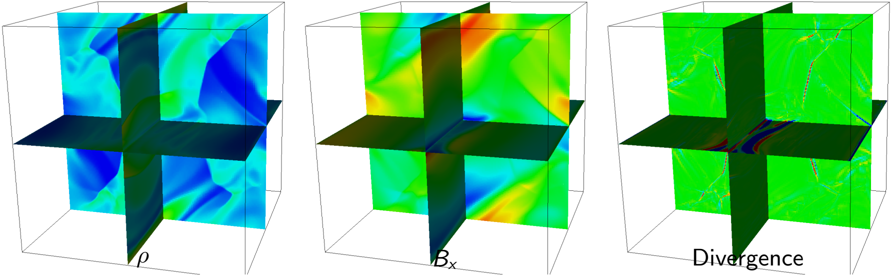

Orszag-Tang vortex in 3D

$t = 0.5$

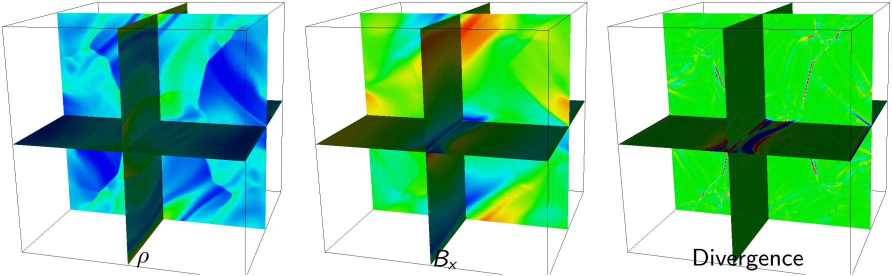

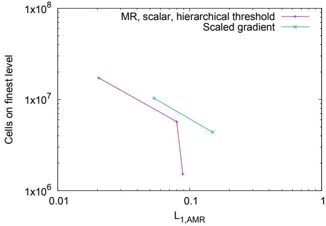

- Error is evaluated in ρ only
- SG and MR with hierarchical threshold applied to ρ, ρu, ρv

Conclusions

- For the first time, wavelet-based multi-resolution has been implemented as refinement criterion in a general and parallel structured AMR framework.
- An approach has been devised to quantify the efficiency of mesh adaptation criteria using the adaptation error for arbitrary problems.

Conclusions

- For the first time, wavelet-based multi-resolution has been implemented as refinement criterion in a general and parallel structured AMR framework.
- An approach has been devised to quantify the efficiency of mesh adaptation criteria using the adaptation error for arbitrary problems.
- Initial tests for shock-capturing FV method for Euler equations and ideal MHD equations are very promising:
  - In complex configurations, involving discontinuities as well as rarefactions, the MR criterion is shown to be significantly more effective than currently used criteria.
  - In rare situations, consisting primarily of global discontinuities, the SG criterion can be most efficient; however, the MR criterion can be tuned to give almost comparable performance.

Conclusions

- For the first time, wavelet-based multi-resolution has been implemented as refinement criterion in a general and parallel structured AMR framework.
- An approach has been devised to quantify the efficiency of mesh adaptation criteria using the adaptation error for arbitrary problems.
- Initial tests for shock-capturing FV method for Euler equations and ideal MHD equations are very promising:
  - In complex configurations, involving discontinuities as well as rarefactions, the MR criterion is shown to be significantly more effective than currently used criteria.
  - In rare situations, consisting primarily of global discontinuities, the SG criterion can be most efficient; however, the MR criterion can be tuned to give almost comparable performance.
- Next steps will be to
  - Replace the SAMR interpolation with the wavelet prediction for consistency (where possible)
  - Test more complex MHD cases in combination with the MR criteria

References I

[Bell et al., 1994] Bell, J., Berger, M., Saltzman, J., and Welcome, M. (1994). Three-dimensional adaptive mesh refinement for hyperbolic conservation laws. *SIAM J. Sci. Comp.*, 15(1):127–138.

[Berger, 1986] Berger, M. (1986). Data structures for adaptive grid generation. *SIAM J. Sci. Stat. Comput.*, 7(3):904–916.

[Berger and Rigoutsos, 1991] Berger, M. and Rigoutsos, I. (1991). An algorithm for point clustering and grid generation. *IEEE Transactions on Systems, Man, and Cybernetics*, 21(5):1278–1286.

[Dedner et al., 2002] Dedner, A., Kemm, F., Kröner, D., Munz, C.-D., Schnitzer, T., and Wesenberg, M. (2002). Hyperbolic divergence cleaning for the MHD equations. *J. Comput. Phys.*, 175:645–673.

[Harten, 1995] Harten, A. (1995). Multiresolution algorithms for the numerical solution of hyperbolic conservation laws. *Commun. Pur. Appl. Math.*, 48:1305–1342.

[Rousell et al., 2003] Rousell, O., Schneider, K., Tsigulin, A., and Bockhorn, H. (2003). A conservative fully adaptative multiresolution algorithm for parabolic PDEs. *J. Comput. Phys.*, 188:493–523.

Clustering by signatures

				x	x	x	x	x	x	6
				x	x	x	x	x	x	6
			x	x	x					3
	x	x	x							3
	x	x								2
	x	x								2
	x	x								2
										0
	x	x								2
	x	x								2
Υ	6	6	2	3	2	2	2	2	2	

Υ Flagged cells per row/column

Δ Second derivative of Υ, $\Delta = \Upsilon_{\nu+1} - 2\,\Upsilon_\nu + \Upsilon_{\nu-1}$

Technique from image detection: [Bell et al., 1994], see also [Berger and Rigoutsos, 1991], [Berger, 1986]

Clustering by signatures

				x	x	x	x	x	x	6
				x	x	x	x	x	x	6
			x	x	x					3
	x	x	x							3
	x	x								2
	x	x								2
	x	x								2
										0
	x	x								2
	x	x								2
Υ	6	6	2	3	2	2	2	2	2	

Υ Flagged cells per row/column

Δ Second derivative of Υ, $\Delta = \Upsilon_{\nu+1} - 2\,\Upsilon_\nu + \Upsilon_{\nu-1}$

Technique from image detection: [Bell et al., 1994], see also [Berger and Rigoutsos, 1991], [Berger, 1986]

Clustering by signatures

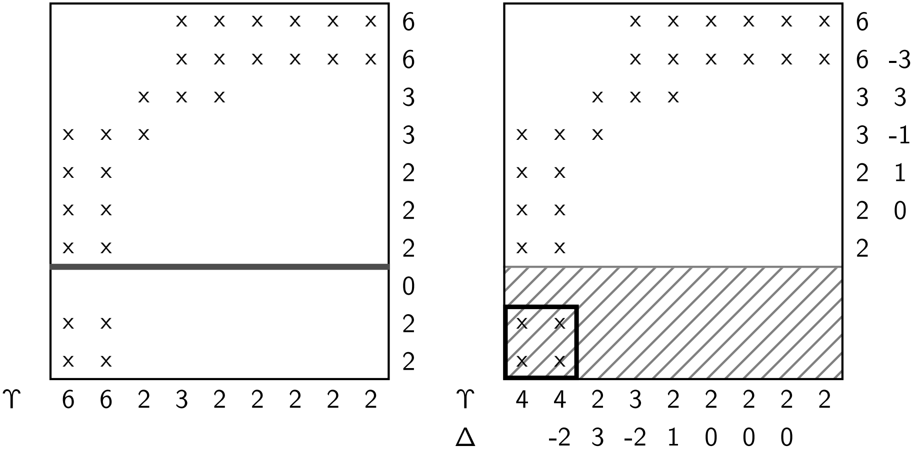

Υ Flagged cells per row/column

Δ Second derivative of Υ, $\Delta = \Upsilon_{\nu+1} - 2\,\Upsilon_{\nu} + \Upsilon_{\nu-1}$

Technique from image detection: [Bell et al., 1994], see also [Berger and Rigoutsos, 1991], [Berger, 1986]

Clustering by signatures

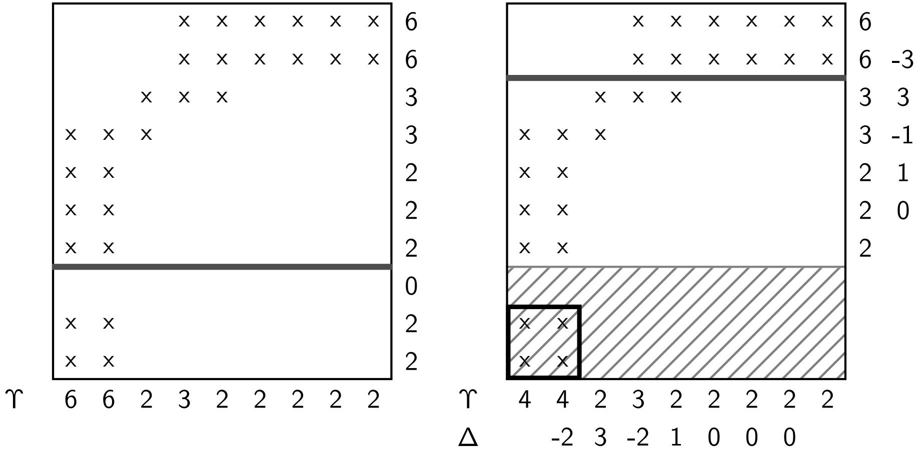

Υ Flagged cells per row/column

Δ Second derivative of Υ, $\Delta = \Upsilon_{\nu+1} - 2\,\Upsilon_{\nu} + \Upsilon_{\nu-1}$

Technique from image detection: [Bell et al., 1994], see also [Berger and Rigoutsos, 1991], [Berger, 1986]

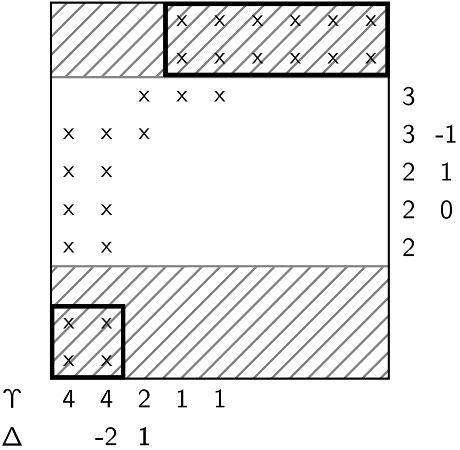

Recursive generation of $\breve{G}_{l,m}$

1. 0 in Υ
2. Largest difference in Δ
3. Stop if ratio between flagged and unflagged cell $> \eta_{tol}$

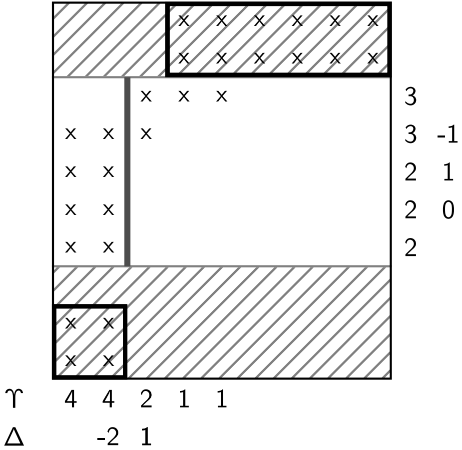

Recursive generation of $\breve{G}_{l,m}$

1. 0 in Υ
2. Largest difference in Δ
3. Stop if ratio between flagged and unflagged cell $> \eta_{tol}$

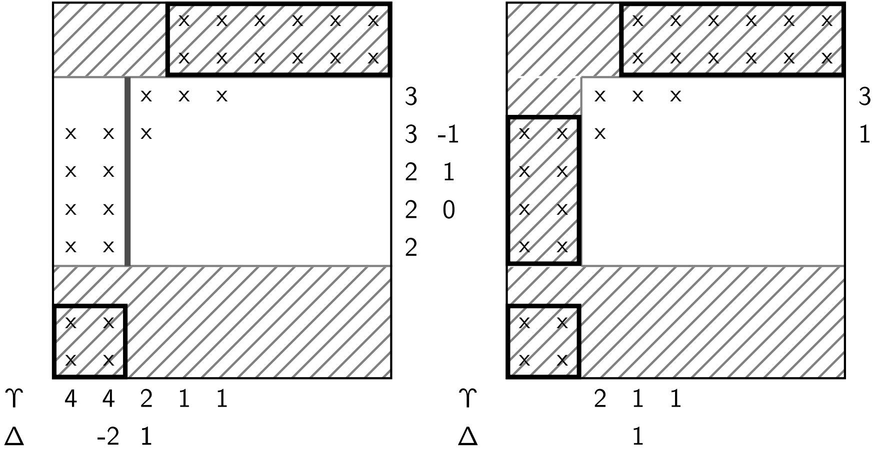

Recursive generation of $\breve{G}_{l,m}$

1. 0 in Υ
2. Largest difference in Δ
3. Stop if ratio between flagged and unflagged cell $> \eta_{tol}$

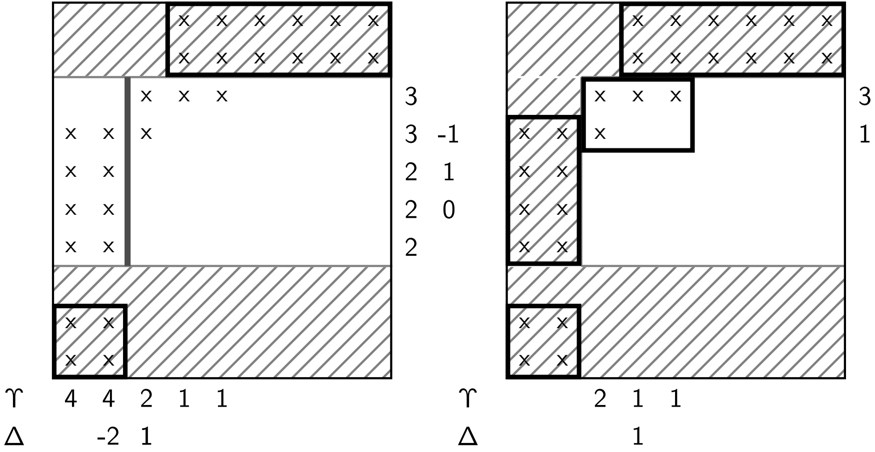

Recursive generation of $\breve{G}_{l,m}$

1. 0 in Υ
2. Largest difference in Δ
3. Stop if ratio between flagged and unflagged cell $> \eta_{tol}$

Parallelization

Rigorous domain decomposition

- Data of all levels resides on same node
- Grid hierarchy defines unique "floor-plan"
- Workload estimation

$$\mathcal{W}(\Omega) = \sum_{l=0}^{l_{\max}} \left[\mathcal{N}_l(G_l \cap \Omega) \prod_{\kappa=0}^{l} r_\kappa \right]$$

Parallelization

Rigorous domain decomposition

- Data of all levels resides on same node
- Grid hierarchy defines unique "floor-plan"
- Workload estimation

$$\mathcal{W}(\Omega) = \sum_{l=0}^{l_{\max}} \left[\mathcal{N}_l(G_l \cap \Omega) \prod_{\kappa=0}^{l} r_\kappa \right]$$

- Parallel operations
  - Synchronization of ghost cells
  - Redistribution of data blocks within regridding operation
  - Flux correction of coarse grid cells
- Dynamic partitioning with space-filling curve

RD (2005). *Adaptive Mesh Refinement - Theory and Applications*, pages 361–372, Springer.

Parallelization

Rigorous domain decomposition

- Data of all levels resides on same node
- Grid hierarchy defines unique "floor-plan"
- Workload estimation

$$\mathcal{W}(\Omega) = \sum_{l=0}^{l_{\max}} \left[\mathcal{N}_l(G_l \cap \Omega) \prod_{\kappa=0}^{l} r_\kappa \right]$$

- Parallel operations
  - Synchronization of ghost cells
  - Redistribution of data blocks within regridding operation
  - Flux correction of coarse grid cells
- Dynamic partitioning with space-filling curve

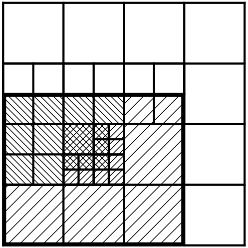

RD (2005). *Adaptive Mesh Refinement - Theory and Applications*, pages 361–372, Springer.

Parallelization

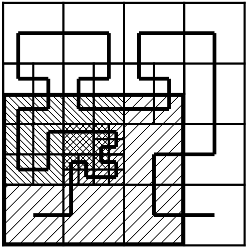

Rigorous domain decomposition

- Data of all levels resides on same node
- Grid hierarchy defines unique "floor-plan"
- Workload estimation

$$\mathcal{W}(\Omega) = \sum_{l=0}^{l_{\max}} \left[\mathcal{N}_l(G_l \cap \Omega) \prod_{\kappa=0}^{l} r_\kappa \right]$$

- Parallel operations
  - Synchronization of ghost cells
  - Redistribution of data blocks within regridding operation
  - Flux correction of coarse grid cells
- Dynamic partitioning with space-filling curve

RD (2005). *Adaptive Mesh Refinement - Theory and Applications*, pages 361–372, Springer.

Parallelization

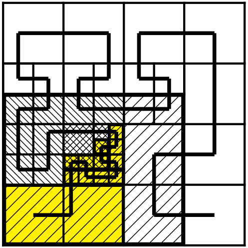

Rigorous domain decomposition

- Data of all levels resides on same node
- Grid hierarchy defines unique "floor-plan"
- Workload estimation

$$\mathcal{W}(\Omega) = \sum_{l=0}^{l_{\max}} \left[\mathcal{N}_l(G_l \cap \Omega) \prod_{\kappa=0}^{l} r_\kappa \right]$$

- Parallel operations
  - Synchronization of ghost cells
  - Redistribution of data blocks within regridding operation
  - Flux correction of coarse grid cells
- Dynamic partitioning with space-filling curve

RD (2005). *Adaptive Mesh Refinement - Theory and Applications*, pages 361–372, Springer.

Parallelization

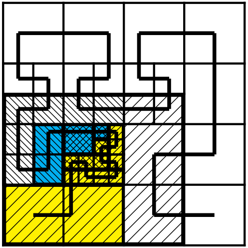

Rigorous domain decomposition

- Data of all levels resides on same node
- Grid hierarchy defines unique "floor-plan"
- Workload estimation

$$\mathcal{W}(\Omega) = \sum_{l=0}^{l_{\max}} \left[\mathcal{N}_l(G_l \cap \Omega) \prod_{\kappa=0}^{l} r_\kappa \right]$$

- Parallel operations
  - Synchronization of ghost cells
  - Redistribution of data blocks within regridding operation
  - Flux correction of coarse grid cells
- Dynamic partitioning with space-filling curve

RD (2005). *Adaptive Mesh Refinement - Theory and Applications*, pages 361–372, Springer.

Parallelization

Rigorous domain decomposition

- Data of all levels resides on same node
- Grid hierarchy defines unique "floor-plan"
- Workload estimation

$$\mathcal{W}(\Omega) = \sum_{l=0}^{l_{\max}} \left[\mathcal{N}_l(G_l \cap \Omega) \prod_{\kappa=0}^{l} r_\kappa \right]$$

- Parallel operations
  - Synchronization of ghost cells
  - Redistribution of data blocks within regridding operation
  - Flux correction of coarse grid cells
- Dynamic partitioning with space-filling curve

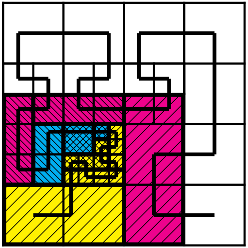

RD (2005). *Adaptive Mesh Refinement - Theory and Applications*, pages 361–372, Springer.

Parallelization

Rigorous domain decomposition

- Data of all levels resides on same node
- Grid hierarchy defines unique "floor-plan"
- Workload estimation

$$\mathcal{W}(\Omega) = \sum_{l=0}^{l_{\max}} \left[\mathcal{N}_l(G_l \cap \Omega) \prod_{\kappa=0}^{l} r_\kappa \right]$$

- Parallel operations
  - Synchronization of ghost cells
  - Redistribution of data blocks within regridding operation
  - Flux correction of coarse grid cells
- Dynamic partitioning with space-filling curve

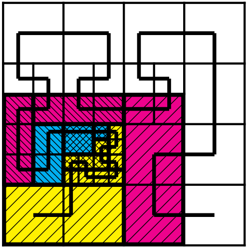

DB: trace8__0.vtk

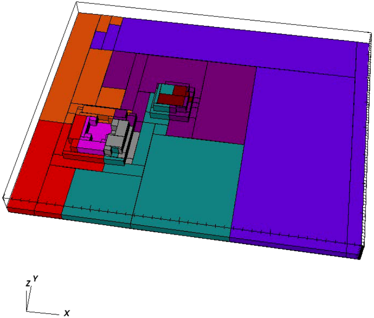

RD (2005). *Adaptive Mesh Refinement - Theory and Applications*, pages 361–372, Springer.